Analysis of $\pi^{\pm}$-^{12}C elastic scattering

O. Dumbrajs and J. Fröhlich
Institut für Theoretische Kernphysik, Universität, D-7500 Karlsruhe 1, Federal Republic of Germany

U. Klein
Institut für Kernphysik and Institut für Experimentelle Kernphysik, Kernforschungszentrum Karlsruhe, D-7500 Karlsruhe 1, Federal Republic of Germany

H. G. Schlaile
Institut für Theoretische Kernphysik, Universität, D-7500 Karlsruhe 1, Federal Republic of Germany
(Received 1 July 1983)

We present an analysis of $\pi^{\pm}$-^{12}C elastic scattering by using a phenomenological ansatz for the pure hadronic amplitude; in addition a careful treatment of Coulomb effects has turned out to be essential. The resulting phase shifts and inelasticity parameters show a smooth behavior in the entire energy region between $T_\pi = 30$ and 230 MeV. The rapid increase of the differential cross sections at backward angles ($T_\pi = 162$ MeV) is discussed in terms of a semiclassical theory of the nuclear glory effect and is well reproduced by using additional information on analytic structure of the π-^{12}C elastic scattering amplitude in the complex t plane.

[NUCLEAR REACTIONS ^{12}C($\pi^{\pm},\pi^{\pm}$)^{12}C, $E = 30$–226 MeV.]

I. INTRODUCTION

There are several good reasons for investigating pion-nucleus elastic scattering, e.g., to obtain information on the isospin structure of the nucleus, to learn something about the off-shell behavior of the hadronic interaction, or to study the applicability of multiparticle scattering theories, etc. The immediate causes for our present analysis of the $\pi^{\pm}$-^{12}C scattering system are as follows:

(i) the large amount of recent pion-carbon data;

(ii) the rapid increase of the differential cross section at backward angles;

(iii) the existence of new measurements in the Coulomb interference region;

(iv) the presentation of pure hadronic phase shifts and inelasticity parameters for further applications.

There exist differential cross sections for π^{+}-^{12}C and π^{-}-^{12}C elastic scattering from 30 to 230 MeV.[1–8] (For an analysis of existing total cross sections see, e.g., Ref. 9.) The large number of $\pi^{\pm}$-^{12}C data is comparable only with the $\pi^{\pm}$-^{16}O system.[10] The phase shift analysis, similar to the analyses of the $\pi^{\pm}$-^{16}O system,[10,11] is then a natural consequence of the available experimental information.

A very interesting feature in the $\pi^{\pm}$-^{12}C data is the rapid increase of the differential cross sections ($T_\pi = 100$ and 165 MeV) at very backward angles; it was impossible until now to give a satisfactory description of this phenomenon.[12]

We will give a semiclassical explanation of this data in Sec. IV, where we also show that a modification of the ansatz of the hadronic amplitude (used in Refs. 10 and 13–18) leads to a satisfactory description of the $\pi^{\pm}$-^{12}C differential cross sections also for the backward angles.

The $\pi^{\pm}$-^{12}C scattering in the Coulomb interference region was measured for the first time below the Δ-resonance energy range only very recently.[4,6] For a theoretical analysis of data (especially in the Coulomb interference region) which have been measured under equal conditions for π^{+} and π^{-} scattering, a careful treatment of various Coulomb effects is necessary in order to extract the maximum of information provided by such measurements.

The importance of such an analysis is increasing, since it has turned out[14] that it might be problematic to add a Coulomb potential to a widely used nonlocal optical potential. In Ref. 19, an attempt has been made to analyze the $\pi^{\pm}$-^{40}Ca data at 64.8 MeV by means of an energy-dependent nonlocal optical model based on the Kisslinger T matrix. It turned out that it was not possible to parametrize π^{+}-^{40}Ca and π^{-}-^{40}Ca scattering with one set of parameters for the pure hadronic amplitude. In addition, the resulting best-fit radii were found to be 0.45 F larger than the corresponding values obtained in electron scattering experiments. We have, therefore, investigated the same scattering system using the methods developed in Refs. 10 and 11. The resulting differential cross sections are in good agreement with experimental data and no indication of isospin violation in the hadronic potential has been found. It is the goal of this paper to present pure nuclear phase shifts and inelasticity parameters for the elastic $\pi^{\pm}$-^{12}C scattering by using the techniques mentioned above. The calculated phase shifts and inelasticity parameters can be used conveniently to test ambitious microscopic theories. In addition, our results can be used in an investigation of distributions of absorbed doses from π^{-} beams, where the Coulomb part is already contained in the considered code.[20]

In Sec. II, we report the main ingredients of the phase

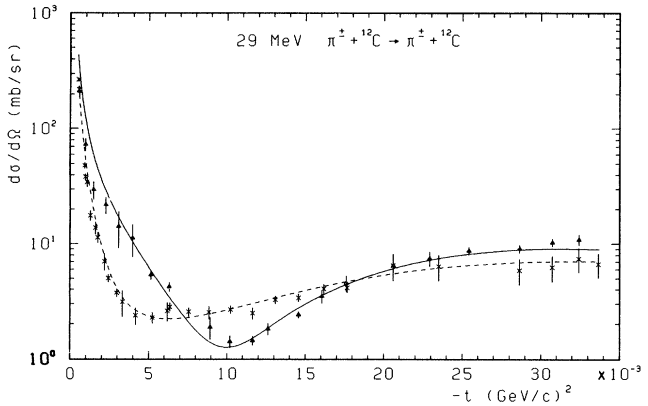

FIG. 1. Differential cross sections for $\pi^{\pm}$-^{12}C elastic scattering. The experimental data (▲—$\pi^{-}{}^{12}$C, ×—$\pi^{+}{}^{12}$C) are taken from Refs. 1–8. The solid (dashed) curves represent π^{-} (π^{+}) ^{12}C differential cross sections resulting from our phase shift analysis.

shift analysis; Sec. III is devoted to the discussion of the results of our analysis. In Sec. IV, we study the compatibility of the $\pi^{\pm}$-^{12}C data at very backward angles with a semiclassical model of the nuclear glory effect and present a satisfactory description of the differential cross sections for all scattering angles. The last section summarizes the analysis of $\pi^{\pm}$-^{12}C scattering.

II. FORMALISM

In order to disentangle the contributions to the elastic differential cross section of $\pi^{\pm}$-^{12}C scattering

$$d\sigma^{\pm}/d\Omega = |f_{\rm tot}^{\pm}|^2 ,$$

we represent the total amplitude $f_{\rm tot}$ as a sum of three parts:

$$f_{\rm tot}^{\pm} = f_H + f_C^{\pm} + f_R^{\pm} . \tag{1}$$

After the partial wave decomposition, the amplitude $f_{\rm tot}^{\pm}$ can be expressed in terms of phase shifts $\delta^{\pm}$ and inelasticity parameters $\eta^{\pm}$,

$$\begin{aligned} f_{{\rm tot},l}^{\pm} &= (\eta_{{\rm tot},l}^{\pm} e^{2i\delta_{{\rm tot},l}^{\pm}} - 1)/2ik \\ &\equiv (e^{2i(\delta_{{\rm tot},l}^{\pm} + i\omega_{{\rm tot},l}^{\pm})} - 1)/2ik , \end{aligned} \tag{2}$$

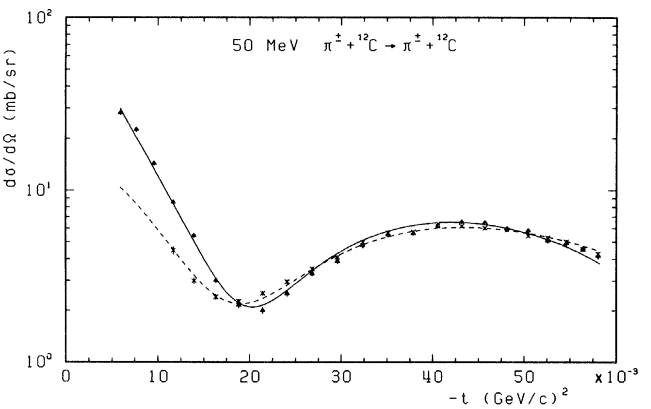

FIG. 2. Same as Fig. 1.

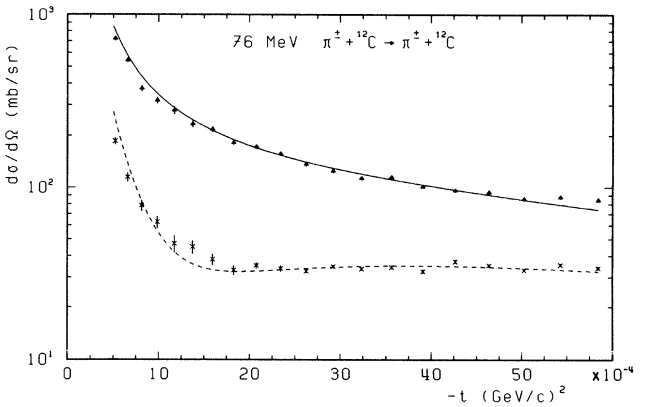

FIG. 3. Same as Fig. 1.

where k is the center-of-mass system momentum. For the pure hadronic amplitude f_H we use a simple complex ansatz,

$$f_H(k^2,t) = f(k^2,0) e^{Bt} \prod_i (1 - t/t_i) , \tag{3}$$

which describes the differential cross section in terms of complex zeros. Here, B (real) and t_i (complex) are free parameters,

$$t = -2k^2(1 - \cos\theta_{\rm c.m.}) ,$$

and $f(k^2,0)$ is the forward scattering amplitude. The number of zeros i is determined by the number of minima or at least expected minima of the differential cross sections. The parametrization of the hadronic amplitude is purely empirical, but it has turned out in many investigations of π-nucleus scattering[10,11,13–18] to be very successful.

$f_C^{\pm}$ is the pure Coulomb amplitude; it can be split into the part $f_C^{\rm point}$, where $\pi^{\pm}$ and ^{12}C are treated as pointlike particles, and $f_C^{\rm ext}$, which represents the contribution from the charge extension of $\pi^{\pm}$ and ^{12}C to the Coulomb amplitude. $f_C^{\rm ext}$ is calculated numerically from the Klein-Gordon equation using the Laguerre polynomial parametrization of Ref. 21 for the ^{12}C charge form factor $F(q^2)$. The pion charge form factor $F_\pi(q^2)$ is taken from Ref. 22 ($q^2 \equiv -t$). The differential cross section at very forward scattering angles is sensitive to relativistic effects

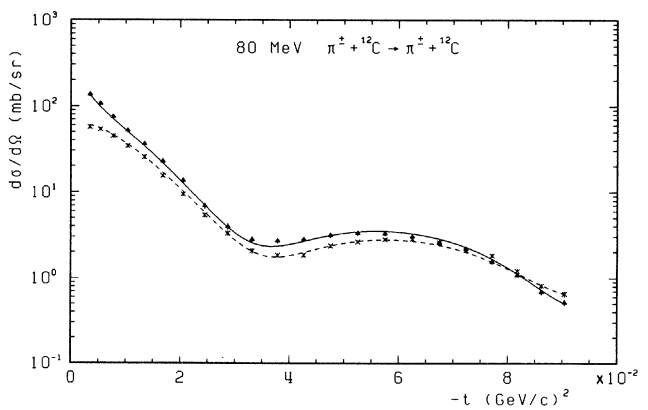

FIG. 4. Same as Fig. 1.

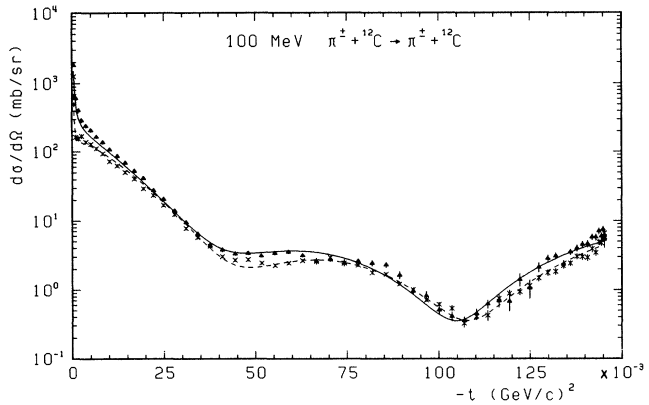

FIG. 5. Same as Fig. 1.

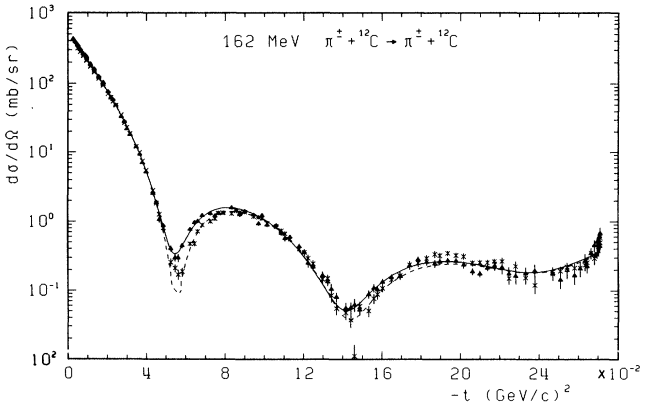

FIG. 7. Same as Fig. 1.

in the point Coulomb amplitude. Therefore, we use the very accurate formulae given in Refs. 14 and 24:

$$f^{\pm}_{C,\text{point}} = f^{(0)}_C + f^{(1)}_C + \Delta f^{(1)}_C \,, \tag{4}$$

where

$$f^{(0)}_C = -\bar{\eta}(2k\sin^2\theta/2)^{-1} e^{-i\bar{\eta}\ln\sin^2\theta/2 + 2i\sigma_0} \,, \tag{5}$$

$$f^{(1)}_C = f^{(0)}_C\left(-\tfrac{1}{2}\pi\bar{\eta}v^2_{\text{lab}}\sin\theta/2 e^{2i(\sigma_{-1/2}+\sigma_0)}\right) \,, \tag{6}$$

$$\Delta f^{(1)}_C = -\sum_{l=0}^{L} f^{(1)}_{C,l} + (2ik)^{-1}\sum_{l=0}^{L}(2l+1)(e^{2i\sigma_\gamma} - e^{2i\sigma_l})P_l \,. \tag{7}$$

$\bar{\eta} = \pm z\alpha v^{-1}_{\text{lab}}$ is the Sommerfeld parameter;

$$\gamma \equiv [(l+\tfrac{1}{2})^2 - z^2\alpha^2]^{1/2}$$

with $z=6$, $\alpha = \frac{1}{137}$; and σ is given by:

$$e^{2i\sigma_{\bar{l}}} = \frac{\Gamma(\bar{l}+1+i\bar{\eta})}{\Gamma(\bar{l}+1-i\bar{\eta})} \,,$$

$$e^{2i\sigma_\gamma} = e^{-i\pi[\gamma-(1/2)-l]}\frac{\Gamma(\gamma+\frac{1}{2}+i\bar{\eta})}{\Gamma(\gamma+\frac{1}{2}-i\bar{\eta})} \,, \tag{8}$$

where $\bar{l}$ is either $-\frac{1}{2}$ or l.

The last contribution $f^{\pm}_R$ to the total amplitude $f^{\pm}_{\text{tot}}$ represents the so-called Coulomb corrections which take into account the modification of the pure hadronic force by the Coulomb interaction. The fact that negative pions are accelerated towards the nucleus while positive pions are slowed down changes not only the momentum of the pions but also their impact parameter.

It has turned out[14] that a semiclassical Wentzel-Kramers-Brillouin (WKB) approximation for the Coulomb corrections[17,18] is not sufficient to satisfactorily describe the differential cross sections for $\pi^{\pm}$-^{40}Ca scattering, especially at the first minimum. The introduction of Coulomb corrections[23] based on the Lippmann-Schwinger formalism has removed these difficulties.

Starting from the two-potential approach of Gell-Mann and Goldberger, the following approximations are made in order to derive simple model-independent equations[23]:

(i) perturbation theory in first order of the Coulomb parameter;

(ii) neglect of "inner" Coulomb corrections;

(iii) Taylor expansion of the pure hadronic half off-shell T matrix around the on-shell value.

The Coulomb corrections are then given in terms of phase shifts

$$(\delta^{\pm}_{R,l} = \delta^{\pm}_{\text{tot},l} - \delta_{H,l} - \delta^{\pm}_{C,l} \;;\; \omega^{\pm}_{R,l} = \omega^{\pm}_{\text{tot},l} - \omega_{H,l})$$

by

$$\delta^{\pm}_{R,l} = \hat{\alpha}^{\pm}_{\bar{l}}\left[\frac{d}{dk}\delta_{H,l} + (\sin 2\delta_{H,l}\cosh 2\omega_{H,l})/2k\right] \,, \tag{9}$$

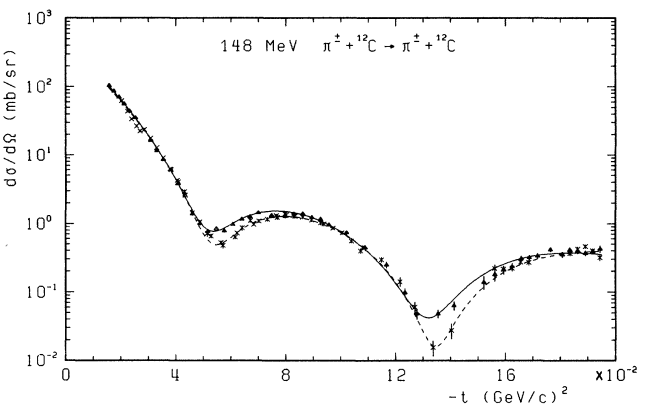

FIG. 6. Same as Fig. 1.

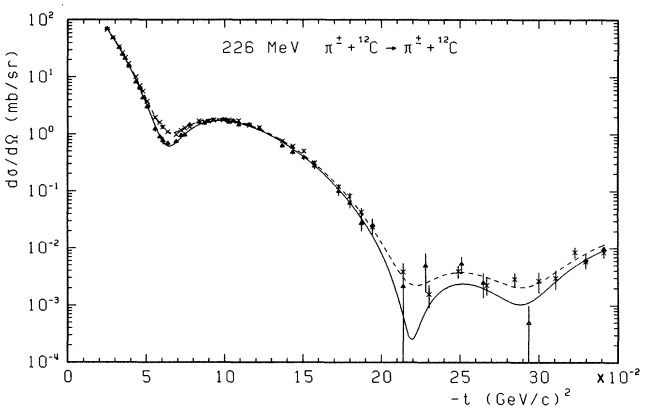

FIG. 8. Same as Fig. 1.

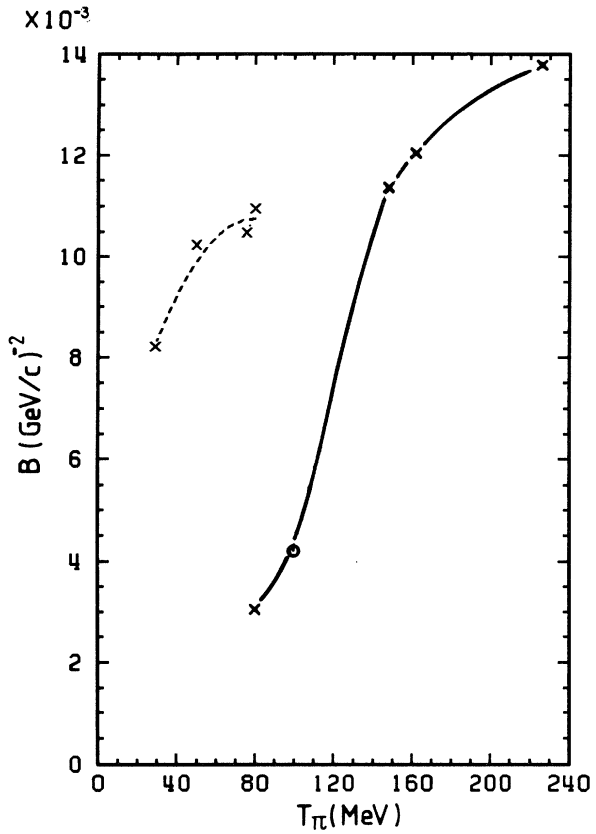

FIG. 9. The energy dependence of the parameter B is marked by crosses. The circle refers to $T_\pi = 100$ MeV. The curves are drawn to guide the eye; the solid curve corresponds to the fits with three complex zeros and the dashed to those with two complex zeros.

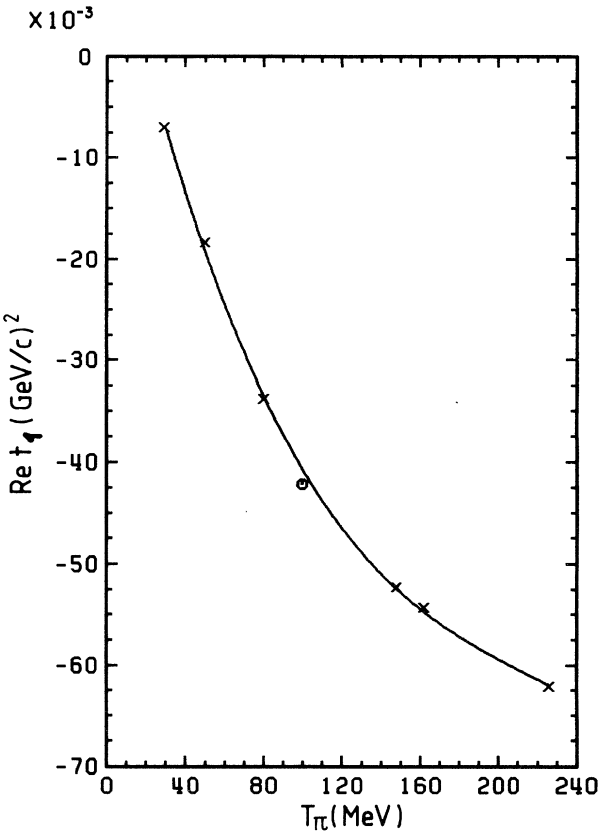

FIG. 10. The energy dependence of free parameters t_i ($i = 1$–3) characterizing the pure hadronic amplitude [Eq. (3)] is marked by crosses; the circles refer to $T_\pi = 100$ MeV. The curves are drawn to guide the eye.

$$\omega_{R,l}^{\pm} = \hat{\alpha}_l^{\pm} \left[\frac{d}{dk} \omega_{H,l} + (\cos 2\delta_{H,l} \sinh 2\omega_{H,l})/2k \right] , \quad (10)$$

with the Coulomb factors

$$\hat{\alpha}_l^{\pm} = \frac{\pm 2 m_\pi z \alpha k}{\pi} P \int_0^\infty dk' \frac{k'^2}{k^2 - k'^2} \times \int_{-1}^{1} dx P_l(x) F(q^2) F_\pi(q^2)/q^2 ; \quad (11)$$

m_π is the pion mass, $q^2 = k^2 + k'^2 - 2kk'x$, and $x \equiv \cos\theta$.

III. PHASE SHIFT ANALYSIS

To determine the pure nuclear phase shifts $\delta_{H,l}$ and inelasticity parameters $\eta_{H,l}$ one must fit free parameters to experimental data. Depending on the energy, i.e., on the number of minima or at least suspected minima in the differential cross sections, we have two or three complex parameters t_i corresponding to zeros of f_H [Eq. (3)]. The slope parameter B must be real to guarantee that the phase variation of the amplitude f_H is given by its nearby zeros. The factor $\exp(-Bt)$ is quite arbitrary and may be replaced by any other smoothly decreasing function of t. This special choice allows one to perform the partial wave decomposition analytically. In addition, we have treated the forward scattering amplitude $f(k^2,0)$ as a complex free parameter. Although it is possible to determine the imaginary part of $f(k^2,0)$ from the total cross sections via the optical theorem, and the real part of $f(k^2,0)$ by using a dispersion relation for the forward scattering amplitude,[11,13] we will use this information only as a reference point for our results to illuminate their quality.

To investigate a broad energy region of the elastic $\pi^{\pm}$-^{12}C scattering, we use experimental data in the range $T_\pi = 29$–226 MeV. Around 30 MeV there exist data from two different measurements, the π^+-^{12}C data[1] at 28.4 MeV, and the π^--^{12}C data[2] at 29 MeV. The lowest energy at which π^+-^{12}C and π^--^{12}C data have been obtained recently under equivalent experimental conditions is 50 MeV.[3] The Karlsruhe group[4] has presented new $\pi^{\pm}$-^{12}C data at 75.6 MeV, where for the first time the Coulomb interference region ($8° < \theta_{\text{c.m.}} < 25°$) has been investigated far below the Δ resonance energy. In addition, at lower energies there exist very recent data on π^+-^{12}C at 80 MeV (Ref. 5) and at 100 MeV (Ref. 6). At higher energies, we have used two data sets from Ref. 7 (148 MeV) and Ref. 8 (162 and 226 MeV). It is worthwhile to point out that at 100 and 162 MeV the measurements have been performed over a broad scattering angle region. At both energies, a rapid increase of the differential cross section

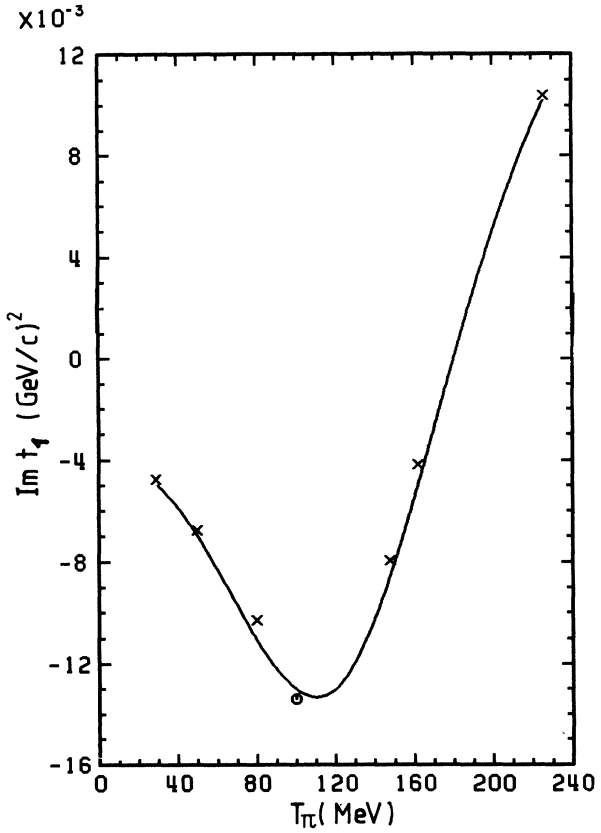

FIG. 11. Same as Fig. 10.

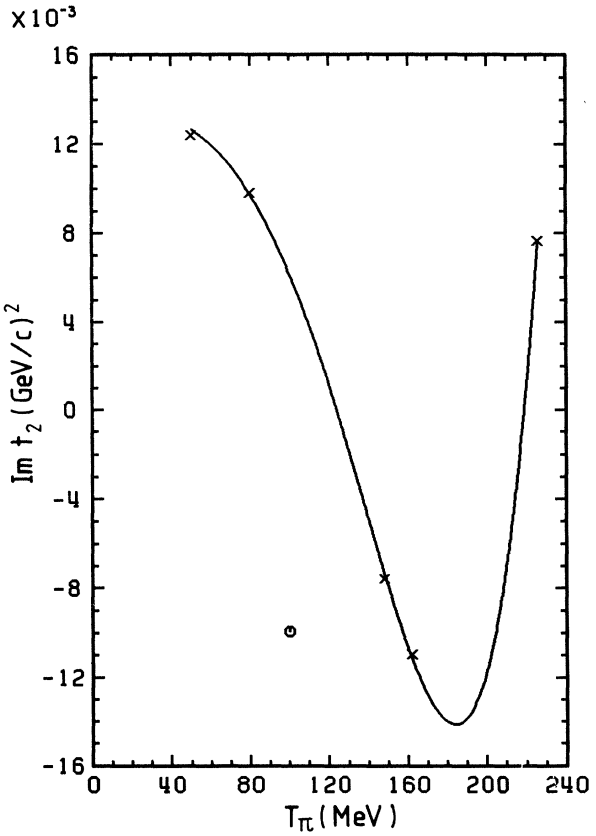

FIG. 13. Same as Fig. 10.

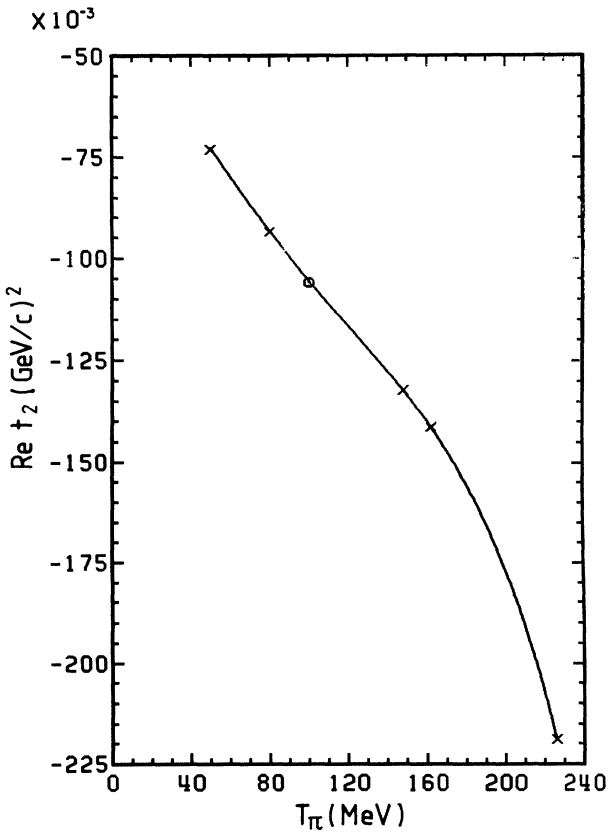

FIG. 12. Same as Fig. 10.

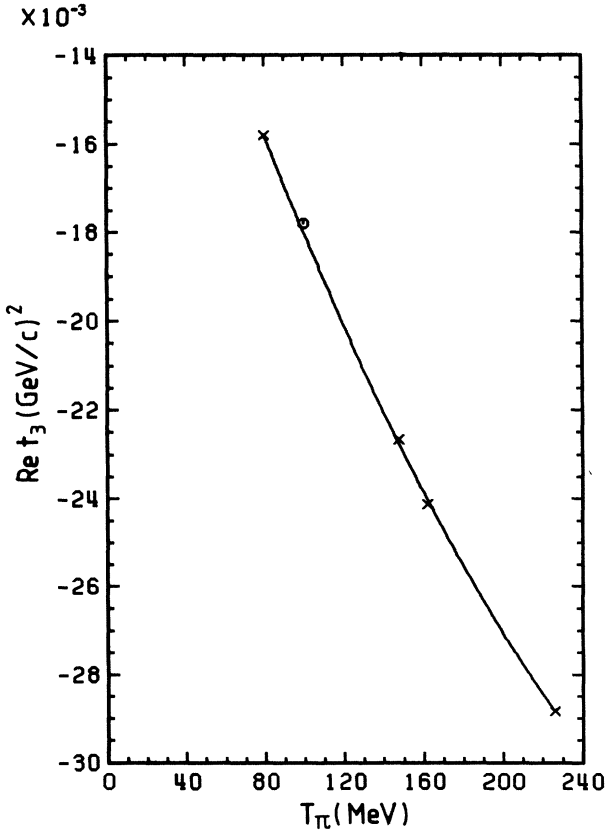

FIG. 14. Same as Fig. 10.

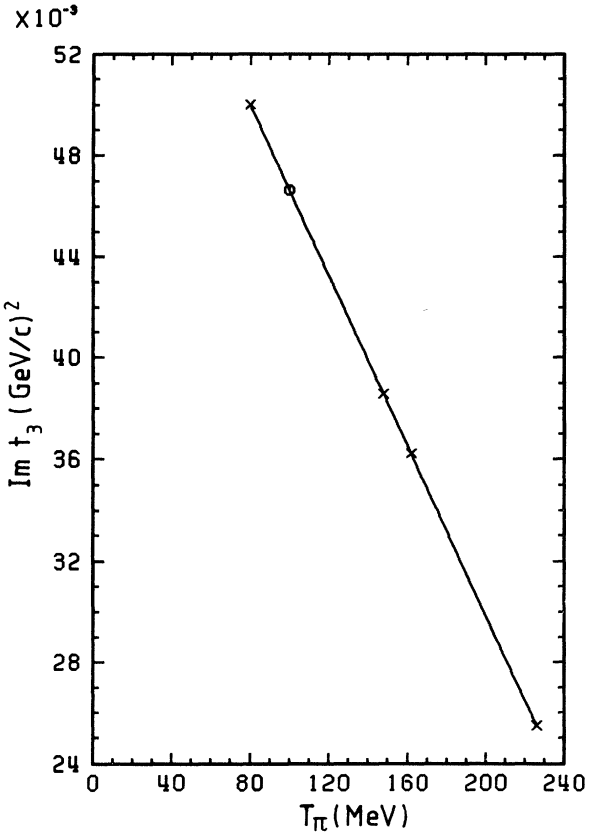

FIG. 15. Same as Fig. 10.

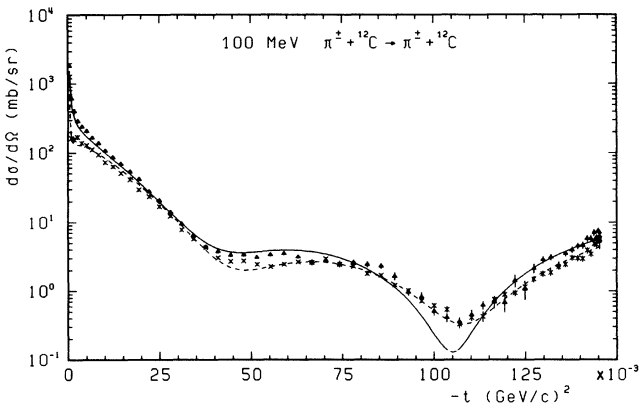

FIG. 16. Differential cross sections for $\pi^{\pm}$-^{12}C elastic scattering at $T_\pi = 100$ MeV. The experimental data are taken from Ref. 6. The solid (dashed) curve is a prediction for π^- (π^+) ^{12}C differential cross sections by fixing the free parameter $\mathrm{Im}t_2$ at the expected value 6×10^{-3} (GeV/c)^2 (see Fig. 13).

around $\theta_{\mathrm{c.m.}} = 180°$ has been observed. Present theoretical calculations[12] (162 MeV) disagree drastically with the data at backward angles. We discuss a semiclassical picture of backward scattering as well as propose another treatment of this problem in Sec. IV.

We analyzed six differential cross sections, i.e., π^+-^{12}C and π^--^{12}C cross sections at three energies, in one χ^2-fit procedure. The 10% normalization error of experimental data is included in the analysis. We start the fitting at the three highest energies (226, 162, and 148 MeV) considered. In order to test the continuity in the values of the parameters, we next take three energies one step lower, i.e., at 162, 148, and 100 MeV, and so on. We have fitted the 80 MeV data with two and three zeros in f_H to guarantee a smooth energy behavior of our free parameters also at lower energies. The parameters B, t_i, and $f(k^2,0)$ are mainly determined by different parts of the data; as a consequence their errors are mostly uncorrelated.

The results of our fits as well as the experimental data on elastic $\pi^{\pm}$-^{12}C scattering are shown in Figs. 1–8. The resulting values of parameters B and t_i are displayed in Figs. 9–15. It is evident from Fig. 9 that we have fitted the differential cross sections at 80 MeV with three and two zeros. The difference between the two values of B can be understood from the simple prescription[18]

$$B \rightarrow B - \mathrm{Re}(1/t_3)\,, \tag{12}$$

where the imaginary part of t_3 is neglected. At $T_\pi = 76$ MeV, the differential cross sections have been measured only for small scattering angles which allow only the determination of B and not t_i. Therefore, we have fixed t_1 and t_2 at their expected (interpolated) values.

We would like to note here that, to our knowledge, it was the first time that a satisfactory description of the elastic π^+-^{12}C scattering was achieved over such a large energy region as that shown in Figs. 1–8. Apart from the imaginary part of the second zero t_2 at 100 MeV, all other parameters B and t_i show a smooth behavior over the entire energy region. It is not possible to obtain agreement with the experimental data that is as good as at all other energies by simply changing the sign of $\mathrm{Im}t_2$ (100 MeV). Because of the broad energy region investigated, we are in principle able to quite accurately determine the parameters of f_H at a prechosen energy (between two neighboring measurements). We have, therefore, fixed $\mathrm{Im}t_2$ (100 MeV) at 6×10^{-3} (GeV/c)^2; the resulting differential cross sections are shown in Fig. 16. It is impossible to remove the discrepancies between the experimental data and our analysis without destroying the energy behavior of $\mathrm{Im}t_2$.

On the basis of statistical errors we obtain an overall

TABLE I. The values of parameters entering into the forward dispersion relation [Eqs. (13)–(15)].

Nucleus	$A^{(+)}$ (F)	$\sigma_{\pi A}(\infty)$ (b)	B_A (MeV b^2)	$B_0^{(+)}$ (F^3)	A_1 (F^3)	$\omega_N f_{\mathrm{eff}}^{(+)2}$ (MeV)
^{4}He	$-0.138+0.04i$	0.071	4.79	-0.18	$0.42+0.06i$	-4
^{6}Li	$-0.183+0.055i$	0.100	7.71	-0.39	$0.67+0.12i$	-1
^{12}C	$-0.451+0.132i$	0.200	25.7	-0.49	$1.54+0.34i$	22
^{16}O	$-0.545+0.154i$	0.260	38.0	-0.67	$0.72+0.29i$	-37
^{40}Ca	$-1.4\ \ +0.38i$	0.64	103.	-1.67	$1.12+1.71i$	-51

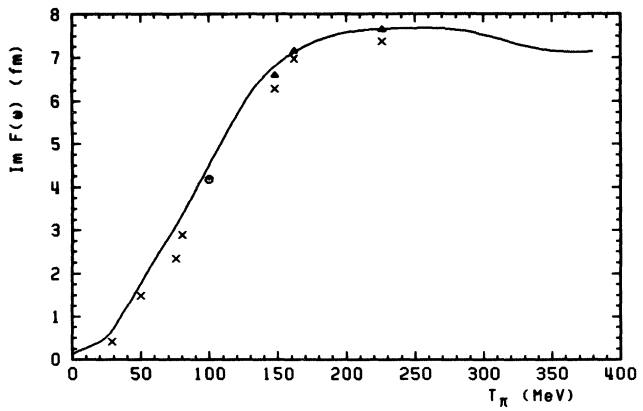

FIG. 17. Imaginary part of the forward scattering amplitude $F(\omega)$. The crosses and the circles are results of our phase shift analysis; the triangles show the values obtained with the use of the improved hadronic amplitude (see Sec. IV). The solid curve is taken from Ref. 9 and represents $\mathrm{Im}F(\omega)$ resulting from a fit to the $\pi^{\pm}$-^{12}C total cross sections.

value of χ^2 per data point equal to 3.25 for all differential cross sections considered. Systematic errors have been included in our analysis as fitting parameters and stay between their values presented in the corresponding experimental papers. As already mentioned above, we have considered the forward scattering amplitude $f(k^2,0)$ as an additional free complex parameter. To compare the values of our free parameter $f(k^2,0)$ with theoretical results, we briefly recall dispersion relations used to determine $\mathrm{Re}f(k^2,0)$. In the equations given below, we write $F(\omega)$ for $f(k^2,0)$, to be consistent with the notation of Refs. 9 and 11:

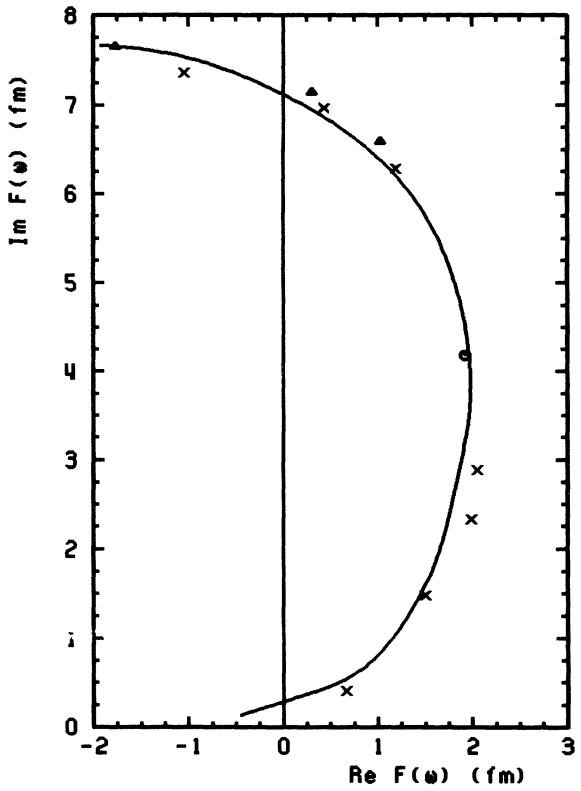

FIG. 19. Argand diagram of the forward scattering amplitude $F(\omega)$. The crosses and the circles are results of our phase shift analysis and the triangles show the values obtained with the improved hadronic amplitude (see Sec. IV). The solid curve is taken from Ref. 9 and represents the results of a dispersion relation calculation for $\mathrm{Re}F(\omega)$.

$$\mathrm{Re}F(\omega)=\mathrm{Re}A^{(+)}-2k^2m_\pi^2\omega^{-2}\omega_N f_{\mathrm{eff}}^{(+)2}$$
$$+2k^2\pi^{-1}\left[P\int_{2\omega_n}^{m_\pi+\omega_n}\frac{\omega' d\omega'}{k'^2(\omega'^2-\omega^2)}\frac{\omega'-2\omega_n}{m_\pi-2\omega_n}\mathrm{Im}F_{\mathrm{th}}(\omega')+P\int_{m_\pi+\omega_n}^{\infty}\frac{\omega' d\omega'}{k'^2(\omega'^2-\omega^2)}\mathrm{Im}F(\omega')\right], \tag{13}$$

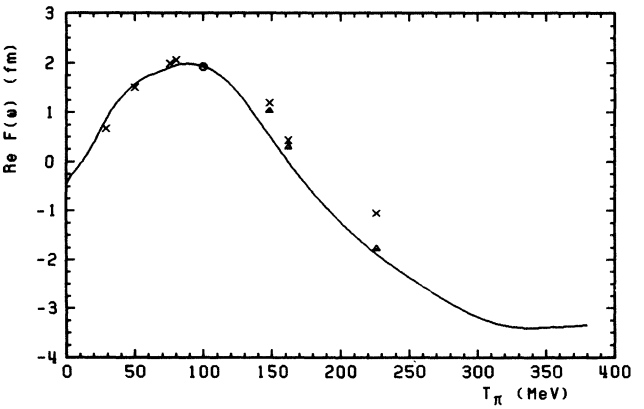

FIG. 18. Real part of the forward scattering amplitude $F(\omega)$. The crosses and the circles are results of our phase shift analysis and the triangles show the values obtained with the improved hadronic amplitude (see Sec. IV). The solid curve is taken from Ref. 9 and represents the results of a dispersion relation calculation for $\mathrm{Re}F(\omega)$.

where F_{th} is the threshold expansion of F

$$F_{\mathrm{th}}=F_0+3F_1\ ,\quad F_1=k^2(A_1^{-1}-ik^3)^{-1}\ , \tag{14}$$

$$F_0=[1-ik(A^{(+)}+k^2B_0^{(+)})]^{-1}(A^{(+)}+k^2B_0^{(+)})\ , \tag{15}$$

ω is the total pion lab energy ($\omega=m_\pi+T_\pi$). The dispersion relation is subtracted at threshold, where F is given by the scattering length

$$A^{(+)}=(-0.451+i0{\cdot}132)F\ ;$$

ω_n is the neutron emission threshold given by $\omega_n=18.3$ MeV. Above $\omega=10m_\pi$, we have parametrized the total cross section by

$$\sigma(\omega>10m_\pi)=\sigma_{\pi A}(\infty)+(B_A/\omega)^{1/2}\ . \tag{16}$$

The parameters $\omega_N f_{\mathrm{eff}}^{(+)}$, A_1, B_0, and B_A, as well as the scattering length $A^{(+)}$ and $\sigma_{\pi A}(\infty)$, are listed in Table I. For a comparison with other nuclei, we also give the values for ^{4}He, ^{6}Li, and ^{16}O from Ref. 9, as well as the values for ^{40}Ca determined in Ref. 15. A detailed descrip-

TABLE II. Pure hadronic phase shifts δ_l obtained from our analysis.

E/l	0	1	2	3	4	5	6	7	8	9
30	−14.58	6.07	1.84	0.100						
50	−17.06	12.70	6.50	0.72	0.05					
75.6	−7.37	13.69	13.22	2.23	0.24	0.02				
80.0	−7.28	16.15	15.26	2.66	0.32	0.03				
100	21.80	24.19	22.20	5.30	0.48	0.03				
148	55.78	−62.64	24.25	11.30	2.59	0.55	0.10	0.01		
162	62.35	−63.80	15.42	7.45	1.61	0.36	0.07	0.01		
226	37.49	−89.24	−31.28	−16.56	−7.19	−2.84	−1.02	−0.32	−0.09	−0.02

tion of Eqs. (13)—(15) can be found in Refs. 9 and 11.

The imaginary part of $F(\omega)$, resulting from a fit to the total cross sections, is shown in Fig. 17. The corresponding real part obtained by means of the dispersion relation is displayed in Fig. 18. In addition, we present the Argand diagram of the forward scattering amplitude $F(\omega)$ in Fig. 19.

A comparison of these results with the $f(k^2,0)$ values found from the analysis of the $\pi^{\pm}$-^{12}C differential cross sections is also shown in Figs. 17—19. Although at higher energies (148—226 MeV) there are small deviations from theoretical results, the overall picture in the entire energy region is satisfactory.

In addition, we want to draw attention to the fact that we have used the same parameters for parametrization of π^+-^{12}C and π^--^{12}C differential cross sections. No assumption about violation of isospin invariance of hadronic force was needed. It is obvious that the number of partial waves contributing to the differential cross sections increases with increasing energy. Since our analysis results in a fairly unique set of partial waves, we present the pure hadronic phase shifts and inelasticity parameters in Tables II and III, respectively.

Finally, we make a comment on the differential cross sections at $T_\pi = 162$ and 100 MeV. We have already mentioned that the experimental data increase rapidly at backward angles. It has been impossible until now[12] [and also with the use of our parametrization Eq. (3), see Fig. 7] to describe this feature satisfactorily. A more ambitious parametrization of the differential cross sections which fits even the backward peak accurately is given in the next section.

IV. IMPROVED PARAMETRIZATION OF THE PURE HADRONIC AMPLITUDE

Before turning to the improved description of the pure hadronic amplitude, we first try to answer the following question: Is there any theoretical model which satisfactorily describes the backward peak of the differential cross section?

In the elastic scattering of α particles by spin zero nuclei, a similar enhancement of the differential cross sections had been observed a long time ago. Bryant and Jarmie[25] described this effect, the so-called nuclear glory effect, within a semiclassical model. They assumed that the beam particles which graze the surface of the target nuclei have an appreciable amplitude for being trapped near the surface, traveling some way along the surface and then emerging as elastically scattered particles. Assuming uniform illumination of the nucleus, all particles which emerge at backward angles travel the same distance on the surface of the target. As a consequence, constructive interference of these scattered particles produces the large increase of the differential cross sections at backward angles.

The results of Ref. 25 for spin-zero—spin-zero scattering were already obtained in the review article[26] on semiclassical scattering. The approximations inherent in the nuclear glory scattering are extensively discussed there and will be only listed in the next lines. They start with the partial wave decomposed hadronic amplitude

$$f_H(\theta) = \sum_{l=0}^{\infty} (2l+1)[(e^{2i\delta_l}-1)/2ik]P_l(\cos\theta) , \qquad (17)$$

TABLE III. Pure hadronic inelasticity parameters η_l obtained from our analysis.

E/l	0	1	2	3	4	5	6	7	8	9
30	0.74	1.00	0.99	1.00						
50	0.65	0.86	0.89	0.98	1.00					
75.6	0.28	0.70	0.79	0.94	0.99	1.00				
80.0	0.16	0.60	0.73	0.92	0.99	1.00				
100	0.20	0.08	0.63	0.81	0.98	1.00				
148	0.19	0.03	0.23	0.43	0.76	0.94	0.99	1.00		
162	0.16	0.11	0.09	0.29	0.67	0.90	0.98	1.00		
226	0.12	0.04	0.06	0.21	0.47	0.73	0.90	0.97	0.99	1.00

where the inelasticity parameter is set equal to one, and use the following approximations:

(i) the phase shift δ_l is replaced by its WKB-approximate value;

(ii) the Legendre polynomial is replaced by the asymptotic expression

$$P_l(\cos\theta)\approx\cos^l\theta J_0[(l+\tfrac{1}{2})\theta]\ ; \tag{18}$$

(iii) the summation of partial wave amplitudes in Eq. (17) is replaced by an integral ($\sum_l \to \int dl$). As a consequence, the differential cross sections can be parametrized by the simple formula

$$\frac{d\sigma}{d\Omega}=AJ_0^2(u)\ , \tag{19}$$

where A is a normalization constant, J_0 is the Bessel function, and

$$u=kR\sin(\pi-\theta)\ . \tag{20}$$

Here R is the so-called interaction radius. The approximations inherent in (19) break down at angles below 155°. Using Eq. (19), Bryant and Jarmie[25] have parametrized differential cross sections for α-nuclei scattering quite successfully. A similar effect in the high energy pion-nucleon scattering has been also investigated. In order to test whether it is possible to describe the π-^{12}C backward peak in the same manner, we fitted the differential cross sections at $T_\pi=162$ and 100 MeV using Eq. (19). Since this equation is derived without inclusion of Coulomb effects, we sum the π^+ and π^- data and divide them by two. Indeed, we find that one can fit the backward data ($155°<\theta<180°$) at 162 MeV quite successfully with the following values of the parameters: $A=0.52$ mb/sr and $R=2.9$ F. A similar fit to the 100 MeV data is also good. The problem of the strange location of Imt_2 discussed in Sec. III does not occur in this approach due to the presence of the free parameter A in Eq. (19).

If surface absorption is low enough in nuclear glory scattering so that the probability of multiple circumvolutions is non-negligible, one expects periodic resonances in the strength factor A (Ref. 25) corresponding to the circumference of the scatterer being an integral number of wavelengths of the particle in the surface. A detailed experimental study of the backward region in the forthcoming experiment[27] would be quite desirable.

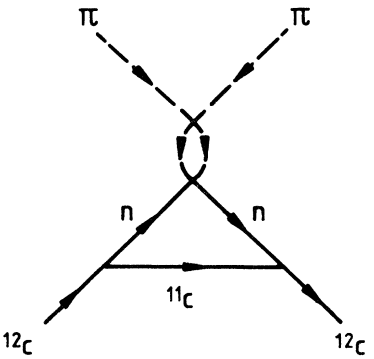

FIG. 20. The graph corresponding to the lowest t-channel anomalous cut in the reaction $\pi+{}^{12}\text{C}\to\pi+{}^{12}\text{C}$. The cut starts at $t_0=0.152$ GeV^2.

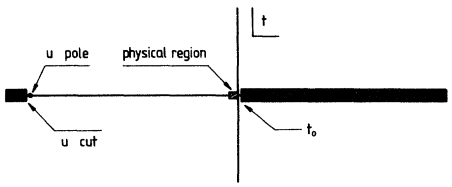

FIG. 21. The analytic structure of the π^{12}C elastic scattering amplitude in the t plane. The scale corresponds to $T_\pi=162$ MeV: $t_{u\ \text{cut}}=-7.11$ GeV^2, $t_{u\ \text{pole}}=-7.07$ GeV^2, and the physical region is at $-0.27\lesssim t\lesssim 0$ GeV^2; $t_{2\pi}=0.078$ GeV^2 (not shown) and $t_0=0.152$ GeV^2.

In the present paper, we are primarily interested in a global description of $\pi^{\pm}$-^{12}C scattering. Therefore, we will not pursue this semiclassical description of the backward scattering but will return to our formalism.

The parametrization used,

$$f_H(k^2,t)=f(k^2,0)\exp(Bt)\left[1-\frac{t}{t_1}\right]\left[1-\frac{t}{t_2}\right]\left[1-\frac{t}{t_3}\right], \tag{21}$$

does not take into account analytic properties of the scattering amplitude in the t variable. It is obvious that the inclusion of the information on the analyticity in the t plane can only improve the description of the data. In the t plane, the π^{12}C scattering amplitude has the right-hand (t channel) cut which begins at $t_{2\pi}=4m_\pi^2\approx 0.078$ GeV^2 and corresponds to the 2π exchange. Next comes the anomalous threshold produced by the graph shown in Fig. 20. This threshold is at

$$t_0=4m_n^2-\frac{(m_{^{12}\text{C}}^2-m_{^{11}\text{C}}^2-m_n^2)^2}{m_{^{11}\text{C}}^2}\ . \tag{22}$$

The nearest left-hand (u channel) singularity is the pole owing to the process π^+-^{12}C$\to{}^{12}$N($\pi^-+{}^{12}\text{C}\to{}^{12}$B) situated at

$$t_{u\ \text{pole}}=(m_\pi-m_{^{12}\text{C}})^2-\left[\frac{m_{^{12}\text{N}}+m_{^{12}\text{B}}}{2}\right]^2-2m_{^{12}\text{C}}T_\pi\ . \tag{23}$$

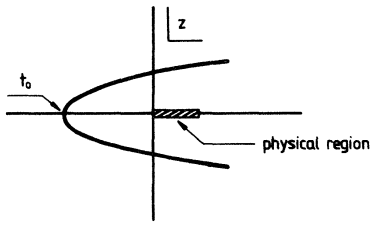

FIG. 22. The analytic structure of the π^{12}C elastic scattering amplitude in the z plane. The images of the u-channel singularities and the cut between $t_{2\pi}$ and t_0 are not shown. The scale corresponds to $T_\pi=162$ MeV; the physical region is at $0\le z\lesssim 1.21$. $z(t_0)=-\pi^2/4$.

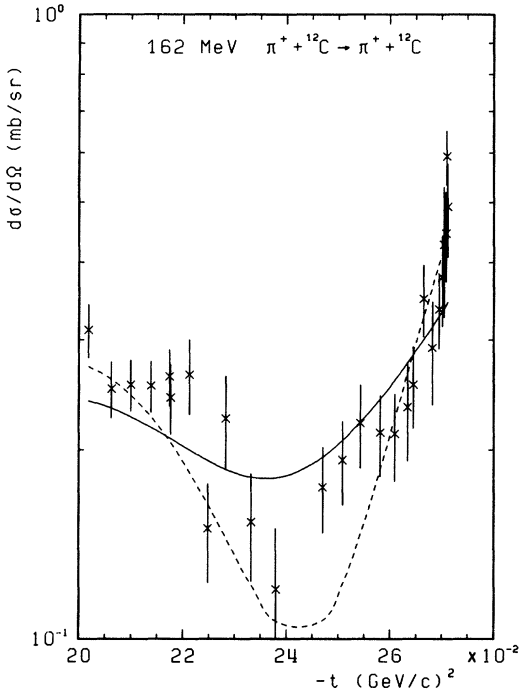

FIG. 23. Differential cross sections at backward angles. The experimental data are taken from Refs. 7 and 8. The solid curve is the result of our phase shift analysis and is equivalent to the results shown in Fig. 7. The dashed curve is obtained with the improved hadronic amplitude (see Sec. IV).

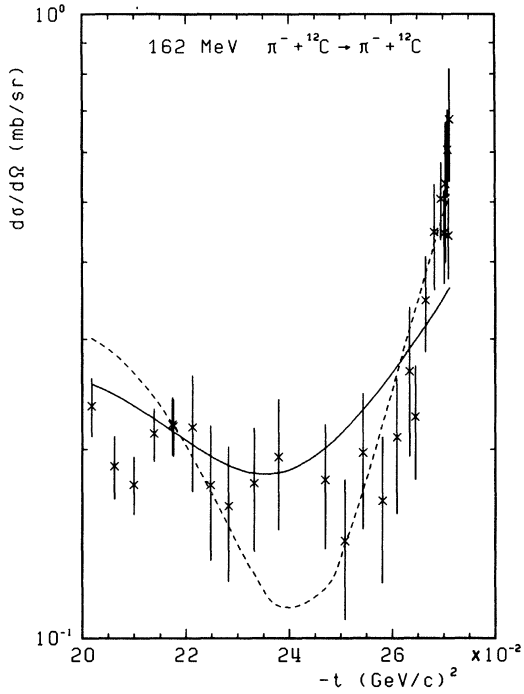

FIG. 24. Same as Fig. 23.

This is followed by the u channel cut due to the process $\pi^+ + {}^{12}C \rightarrow p + {}^{11}C$($\pi^- + {}^{12}C \rightarrow n + {}^{11}B$) starting at

$$t_{u\ \mathrm{cut}} = (m_\pi - m_{{}^{12}C})^2 - \left[\frac{m_p + m_n + {}^{11}B + {}^{11}C}{2}\right]^2 - 2m_{{}^{12}C}T_\pi \ . \tag{24}$$

The resulting analyticity structure of the $\pi^{12}C$ scattering amplitude in the t plane is shown in Fig. 21. It is evident from Fig. 21 that one can expect that the contributions from the left-hand singularities are not important for the purpose of description of data because they are very far from the physical region. Thus, we assume that the only relevant singularity of the $\pi^{12}C$ scattering amplitude in the t plane is the right-hand cut. Here we ignore the 2π-exchange cut which is expected to be weak in comparison with the nuclear structure singularity.

Now one can recall the idea that the best way of representing an analytic function with known analytic properties in the form of a polynomial expansion is to choose a variable which places the "data region" and the cuts on equipotential curves.[28] In our case (only one cut), this variable corresponds to the mapping of the whole cut t plane into the inside of a parabola in the z plane with the focus at the origin[29]

$$z = [\ln(\sqrt{-t/t_0} + \sqrt{-t/t_0 + 1})]^2 \ . \tag{25}$$

The image of the data region coincides with a part of the right half of the real axis and the cut with the boundary of the parabola (Fig. 22).

Now the Laguerre polynomials with an exponential weight function are suitable for making the expansion

$$f_H(k^2,t) = \exp(-\beta z) \sum_{n=0}^{N} a_n L_n(2\beta z) \ , \tag{26}$$

because the region of convergence of this expansion is a parabola with origin as focus.[30] The constant β and coefficients a_n are free parameters.

Taking into account the fact that the data at $T_\pi = 162$ MeV require only two or three zeros, we keep four terms in Eq. (24) and rewrite it in the form

$$f_H(k^2,t) = f(k^2,0)\exp(-\beta z) \times \left[1 - \frac{z}{z_1}\right]\left[1 - \frac{z}{z_2}\right]\left[1 - \frac{z}{z_3}\right] , \tag{27}$$

TABLE IV. The best-fit values of parameters β and z_i in Eq. (27).

T_π (MeV)	β	z_1	z_2	z_3
148	1.3000	$0.3118 + i0.0458$	$0.7013 + i0.0317$	$1.0678 - i0.0864$
162	1.3789	$0.3236 + i0.0241$	$0.7438 + i0.0422$	$1.1422 - i0.2741$
226	2.0360	$0.3622 - i0.0616$	$1.0525 - i0.0004$	$1.3169 - i0.0003$

where z_1, z_2, and z_3 are locations of zeros of the differential cross section in the z plane. The form of Eq. (27) is similar to the form of Eq. (21). However, because of Eq. (25), the dependence of $d\sigma/d\Omega$ on t is now different. The fact that there is a cut in the t plane starting at t_0 is ignored in the parametrization (21) and is built in explicitly in the parametrization (27). The factor $\exp(-\beta z)$ falls slower than exponentially in t allowing in this way for the last multiplier in Eq. (27) to more easily simulate the increase of the backward cross section.

As is evident in Figs. 23 and 24, the use of Eq. (27) instead of Eq. (21) in Eq. (1) (Table IV) has improved the description of the differential cross section for $\pi^{\pm}$-^{12}C elastic backward scattering at $T_\pi = 162$ MeV. Here the quality of the fits at smaller angles has not deteriorated.

As a by-product of this new parametrization, we find that the real part of the forward scattering amplitude is now closer to the values predicted by the dispersion relations. The results for $F(\omega)$ obtained using Eq. (27) are marked in Fig. 18 by triangles.

V. SUMMARY

We have investigated elastic π-^{12}C scattering over a large energy region by analyzing π^+-^{12}C and π^--^{12}C differential cross sections. Using a phenomenological ansatz for the pure hadronic amplitude, we find that a careful treatment of Coulomb effects is needed in order to describe $\pi^{\pm}$-^{12}C data with one set of parameters of the hadronic amplitude. The phase shift analysis presented in Sec. III results in a fairly unique set of partial waves; here all partial waves show a smooth behavior over the entire energy region. Owing to the large energy region considered, we were able to quite accurately determine the parameters of the hadronic amplitude. The rapid increase of the differential cross sections at backward angles can be qualitatively understood in terms of a semiclassical model of the nuclear glory scattering. We have presented in Sec. IV an improved parametrization of the hadronic amplitude which takes into account the analytic structure in the t plane. A good description of experimental data also at the backward angles has been obtained by means of this new ansatz. In comparison with the parametrization of f_H used in Sec. III, the analysis by means of the new ansatz for f_H is more time consuming, because, in order to treat Coulomb corrections, a numerical partial wave decomposition of f_H is unavoidable in contrast to the analytic decomposition in Sec. III.

ACKNOWLEDGMENTS

The authors are grateful to M. Blecher, J. P. Egger, W. Kluge, and B. Saghai for sending us their $\pi^{\pm}$-^{12}C data ($T_\pi = 80$, 100, 76, and 50 MeV) prior to publication. In addition, they wish to thank H. Pilkuhn for many fruitful discussions.

[1]R. R. Johnson *et al.*, Nucl. Phys. A296, 444 (1978).
[2]R. R. Johnson *et al.*, Phys. Lett. 78B, 560 (1978).
[3]G. H. Daw, M.S. thesis, New Mexico State University, 1981.
[4]H. Degitz, Ph.D. thesis, Kernforschungszentrum Karlsruhe, 1983; W. Kluge, private communication.
[5]M. Blecher, private communication.
[6]J. P. Egger, private communication.
[7]J. Piffaretti *et al.*, Phys. Lett. 67B, 285 (1977).
[8]J. Piffaretti *et al.*, Phys. Lett. 71B, 324 (1977).
[9]H. Pilkuhn, N. Zovko, and H. G. Schlaile, Z. Phys. A 279, 283 (1976).
[10]J. Fröhlich, H. G. Schlaile, L. Streit, and H. F. K. Zingl, Z. Phys. A 302, 89 (1981).
[11]S. Ciulli, H. Pilkuhn, and H. G. Schlaile, Z. Phys. A 302, 45 (1981).
[12]M. Hirata, F. Lenz, and M. Thies, SIN Report PR 82-19, 1982.
[13]J. F. Germond and C. Wilkin, Nucl. Phys. A237, 477 (1975).
[14]J. Fröhlich, H. Pilkuhn, and H. G. Schlaile, Phys. Lett. 121B, 235 (1983).
[15]J. Fröhlich, H. Pilkuhn, and H. G. Schlaile, Report TKP 83-6, 1983; Nucl. Phys. (in press).
[16]J. F. Germond and C. Wilkin, Phys. Lett. 67B, 289 (1977).
[17]R. Jäckle, H. Pilkuhn, and H. G. Schlaile, Phys. Lett. 76B, 177 (1978).
[18]J. F. Germond and C. Wilkin, Ann. Phys. (N.Y.) 121, 285 (1979).
[19]S. H. Dam *et al.*, Phys. Rev. C 25, 2574 (1982).
[20]G. Büche and G. Przybilla, Nucl. Instrum. Methods 179, 321 (1981); G. Büche, Radiat. Environ. Biophys. 20, 255 (1982).
[21]O. Dumbrajs, Z. Phys. A 301, 55 (1981).
[22]G. J. Bebeck *et al.*, Phys. Rev. D 17, 1693 (1978).
[23]J. Fröhlich, L. Streit, H. Zankel, and H. F. K. Zingl, J. Phys. G 6, 841 (1980).
[24]H. Pilkuhn, *Relativistic Particle Physics* (Springer, Berlin, 1979).
[25]H. C. Bryant and N. Jarmie, Ann. Phys. (N.Y.) 47, 127 (1968).
[26]K. W. Ford and J. A. Wheeler, Ann. Phys. (N.Y.) 7, 259 (1959).
[27]G. R. Burleson, private communication.
[28]J. L. Walsh, *Interpolation and Approximation by Rational Functions in the Complex Domain* (American Mathematical Society Coll. Publications, 1969).
[29]O. Dumbrajs, Phys. Rev. C 21, 1677 (1980).
[30]H. Pollard, Ann. Math. 48, 358 (1947).